A Reactive Management System for Reliable Power Supply in a Building Microgrid with Vehicle-to-Grid Interaction

メタデータ	言語: eng
	出版者:
	公開日: 2020-01-29
	キーワード (Ja):
	キーワード (En):
	作成者: Kimura, Shoko, Susuki, Yoshihiko, Ishigame, Atsushi
	メールアドレス:
	所属:
URL	http://hdl.handle.net/10466/00016708

PAPER

A Reactive Management System for Reliable Power Supply in a Building Microgrid with Vehicle-to-Grid Interaction

Shoko KIMURA[†a)], *Nonmember*, Yoshihiko SUSUKI[†b)], *Member*, and Atsushi ISHIGAME[†c)], *Nonmember*

SUMMARY We address a BEMS (Building Energy Management System) to guarantee reliability of electric-power supply in dynamic uncertain environments. The building microgrid as the target of BEMS has multiple distributed power sources including a photo-voltaic power system and Electric-Vehicle (EV). EV is regarded as an autonomously-moving battery due to the original means of transportation and is hence a cause of dynamic uncertainty of the building microgrid. The main objective of synthesis of BEMS in this paper is to guarantee the continuous supply of power to the most critical load in a building microgrid and to realize the power supply to the other loads according to a ranking of load importance. We synthesize the BEMS as a reactive control system that monitors changes of dynamic uncertain environment of the microgrid including departure and arrival of an EV, and determines a route of power supply to the most critical load. Also, we conduct numerical experiments of the reactive BEMS using models of power flows in the building and of charging states of the batteries. The experiments are incorporated with data measured in a practical office building and demonstration project of EMS at Osaka, Japan. We show that the BEMS works for extending the time duration of continuous power supply to the most critical load.

key words: energy management system, electric vehicle, building microgrid, reactive system, formal method, linear temporal logic

1. Introduction

This paper addresses a Building Energy Management System (BEMS) to guarantee reliability of electric-power supply in dynamic uncertain environments. A BEMS is the essential component of modern buildings that is responsible for minimizing energy consumption while maintaining occupants' comfort [1]. The impact of resilience and security of BEMS spreads both locally (electrical and mechanical equipment for continuous maintenance of occupants' comfort) and globally (distribution grids and distributed energy systems) [2]. The primary objective of BEMS is that against such impacts it guarantees reliability of energy supply to loads in a building. The so-called reliability in context of energy supply is referred as supplying energy without interruption [3]. Thus, in order to guarantee the supply reliability, it is of basic significance to synthesize a BEMS that monitors and controls complex behaviors of loads (including occupants), commercial grid, and distributed energy resources such as Photo-Voltaic (PV) generation unit and battery.

In-vehicle (or on-board) batteries have attracted a lot of interests for realizing reliable energy management systems [4]. Electrification of automobiles has been drawing attention to solve environmental problems [5] and is expected to provide energy and services into the future power grid [6]. An Electric Vehicle (EV) is regarded as a small-scale power source as well as the original means of transportation and is thus studied from various viewpoints for utilization in electric power grids: see e.g. [7]–[14]. In particular, the so-called Vehicle-to-Grid (V2G) as a coordinated use of in-vehicle batteries for grid's support is considered in [10]–[14]. It should be emphasized from [15] that because every EV has its primary concern of transportation, it is necessary to develop the V2G technology with considering its primary use in transportation. Here, in terms of BEMS, an EV occasionally arrives/leaves the building as the primary means and thus results in a time-varying change of topology of the building microgrid. Thus, it is required to handle the dynamic uncertain nature of the V2G interaction in order to establish the reliable power supply.

Synthesis of EMS in dynamic uncertain environments has been recently studied using the formal method [16]. The authors of [17] apply a framework of model checking [18] to design and implementation of robust smart grids. The authors of [19]–[21] develop methodology and tool for synthesis of reactive control systems from specifications described by Linear Temporal Logic (LTL) [18] and apply them to an aircraft power system. A *reactive system* is a system that maintains an ongoing interaction with its environment, as opposed to computing some final value on termination [22]. LTL is a form used in software engineering to verify the correctness of sequence of discrete states including the temporal concept [18]. By using the form, it is demonstrated in [19]–[21] that a reactive control system is automatically synthesized that dynamically reacts to changes of the uncertain environment of aircraft power system. In [23], by following this, the so-called output leveling of a household power system is achieved with a reactive control system. Also, synthesis and real-time simulation of a reactive control system for reliable hot-water supply in a hospital are reported in [24].

Based on the preceding works, in this paper we synthesize and evaluate a reactive BEMS that handles the configuration change of a building microgrid due to EV and achieves reliable power supply to the most critical load in the building microgrid. The reactive architecture of BEMS is promising for managing dynamic uncertain environments. A rudimentary model of the building microgrid based on a practical

office building [25] is introduced and studied throughout this paper.

The contributions of this paper are two-fold. One contribution is to solve the synthesis problem of reactive BEMS using the methodology and tool in [19]–[21]. The BEMS reacts to changes in the environment of microgrid including arrival and leave of EV, and operates switches in the microgrid in order to archive the continuous supply of power to the most critical load. Although this is one application of the formal method-based synthesis [19]–[21], we show for the first time that the formal method is effective for developing a BEMS with cooperation of EV. The novelty of the work is that we include the utilization of EV as a plug-and-play power source in the synthesis of reactive energy management systems, which does not appear in [23]. The other contribution is to conduct numerical experiments of the reactive BEMS using simulations with measurement data in the practical office building and a V2G demonstration project at Osaka, Japan. Precisely, we conduct a series of numerical simulations in mathematical models of power flows in the microgrid and of charging states of batteries while incorporating time-series data on generation and load as well as EV movement. Thus, we show that the synthesized BEMS works for extending the duration of continuous power supply to the most critical load, which is regarded as a secondary benefit of the reactive BEMS. In particular, the duration under the trip of commercial power source is sufficiently extended by utilizing EV.

The rest of the paper is organized as follows. In Sect. 2, we introduce the building microgrid studied in this paper, and we state the synthesis objective. In Sect. 3, we describe requirements of the grid's management as LTL specifications and presents the synthesis result with a concrete example of control actions. In Sect. 4, we conduct numerical simulations of the synthesized BEMS using the measurement data. Section 5 is the conclusion of this paper with a brief summary.

2. Building Microgrid and Synthesis Objective

In this section, we show the configuration of building microgrid studied in this paper. Next, we introduce the main objective of synthesis of reactive BEMS. For the synthesis objective, a series of requirements of the grid's management is presented.

2.1 Building Microgrid

Figure 1 shows the configuration of building microgrid that we study in this paper. This configuration is based on the practical office building [25]. This grid is connected to a commercial power source G_1 and includes PV (Photo Voltaic power source) G_2, Battery G_3, and EV G_4. The distribution network in the grid links the commercial power source G_1 and the multiple distributed power sources G_i ($i = 2, 3, 4$) to the electric loads denoted as NL, CL, and L. The symbol NL corresponds to a normal load of a showroom in the prac-
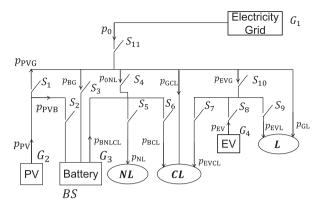

Fig. 1 Building microgrid that we study in this paper. This grid includes a PV (PhotoVoltaic power source), a Battery and an EV (Electric Vehicle). The electric loads are denoted as NL, CL, and L. The symbol NL corresponds to a normal load of a showroom in the practical office building, CL to a critical load of evacuation place and a control server as CPU of BEMS, and L to a critical load of research equipments. The direction of each arrow represents the positiveness of value of the corresponding power. This paper aims to synthesize a supply route of power to the critical loads by changing the status (open or close) of switches denoted as S_i ($i = 1, \ldots, 11$).

Table 1 Meaning of power flows denoted as arrows in Fig. 1.

p_0	Output power from commercial power source
p_{PV}	Output power from PV
p_{PVG}	Power from PV to the distribution network
p_{PVB}	Power from PV to Battery
p_{BG}	Power from the distribution network to Battery
p_{BNLCL}	Power from Battery to NL or CL
p_{0NL}	Power from the distribution network to NL
p_{NL}	Power flowing into NL
p_{BCL}	Power from Battery to CL
p_{GCL}	Power from the distribution network to CL
p_{EVCL}	Power from EV to CL
p_{EVG}	Power from the distribution network to EV
p_{EVL}	Power from EV to L
p_{GL}	Power from the distribution network to L

tical office building, CL to a critical load of evacuation place and a control server as CPU of BEMS, and L to a critical load of research equipments. Thus, the importance of these loads is ranked from CL, L, to NL. This will be addressed below when we consider the grid's management under the trip of commercial power source. In addition, the symbols S_i ($i = 1, \ldots, 11$) denote the switches (circuit breakers) of the building microgrid that determine its configuration and correspond to the actuation devices on the grid's management. Note that the direction of each arrow in Fig. 1 represents the positiveness of value of the corresponding power. Table 1 summarizes the meaning of power flows p_*.

2.2 Synthesis Objective

The main objectives of synthesis of BEMS in this paper are two-fold:

(i) to guarantee the continuous supply of power to the most critical load CL;

(ii) to realize the power supply to the other loads according to their ranking.

Here, it should be noted that the synthesized BEMS needs to work in a dynamically-changing environment. Examples of the environment are the sudden trip of commercial power source, arrival and departure of EV, and failure of any generation unit.

For the synthesis objective, there are fundamental requirements of the grid's management and of the power sources that need to be taken into account:

(iii) If commercial power source G_1 is tripped, then any distributed power source in the grid is disconnected from G_1. This is a practical regulation listed in the Japanese grid code [26], which is related to safety of technicians repairing G_1.

(iv) Under the tripped case, no mixing of electricity from any two power sources is allowed. This appears in [21] so that any problem on synchronization of AC power sources can be avoided.

(v) The grid-connected inverter for PV G_2 is of grid-feeding type [27], and the inverters for Battery G_3 and EV G_4 are of grid-forming type [27]. Hence, G_2 becomes out of operation if no other power source is available in the grid, while G_3 and G_4 are capable of operating even if no other source is available.

(vi) PV G_2, which is the renewable-based power source in the grid, is utilized maximally. This leads to reduction of amount of power supplied from commercial power source G_1 that is sometimes costly. For this, under the trip of G_1, G_2 can supply power to G_3 (that is, charging of Battery from PV) as denoted by p_{PVB} in Fig. 1.

(vii) If any power source is out of operation, then it should be disconnected from the grid. This is required in order to prevent any flow of power into a source, which possibly causes its unintended damage.

According to the above requirements and load ranking, we will introduce in Sect. 3.2 a series of temporal logic specifications that describe supply routes of power from a source to a load.

3. Synthesis of Reactive Management System by Linear Temporal Logic

In this section, based on the methodology and tool proposed in [19]–[21], we synthesize a reactive EMS for the building microgrid that archives the objectives in Sect. 2.2.

3.1 Summarized Theory

First of all, we summarize the methodology and tool in [19]–[21] for automatic generation of reactive control systems from temporal logic specifications. A problem on synthesis of a reactive control system (i.e. a controller that reacts to a dynamic, *a priori* unknown environment) is presented in the following LTL specification φ of assume-guarantee form

[19]–[21]:

$$\varphi = \varphi_e \rightarrow \varphi_s \tag{1}$$

where φ_e is the conjunction of LTL specifications that characterize assumptions on the environment, and φ_s is the conjunction of LTL specifications that characterize the system requirements. Please refer to Appendix A for syntax of LTL. The synthesis problem can be regarded as a two-player game between the environment and controlled plant [19]–[21]. For a subset of LTL called Generalized Reactivity (1) (GR(1)), the problem can be solved in polynomial time [28]. Given a GR(1) specification, the temporal logic planning toolbox, called `TuLip`, automatically generates a finite automaton that represents a reactive control system [29], which will be used in this paper.

3.2 Formal Specifications with LTL

Next, we describe the requirements in Sect. 2.2 and supply routes for every load as LTL specification. To do so, let us define the boolean variables g_i to represent the health status of the power sources G_i ($i = 1, \ldots, 4$). The condition $g_i = 1$ implies that G_i can supply power, which we call *healthy*, and $g_i = 0$ implies that G_i cannot supply power, which we call *unhealthy*. Also, the boolean variable BS is defined to represent whether or not the State of Charge (SOC) of Battery is within its available range; $BS = 0$ implies the SOC deviates from the range. That is to say, Battery can supply power to a load only if both g_3 and BS coincide with 1. The status of the power sources depends on the dynamic analog environment surrounding the building. In this sense, G_i and BS are called the *environment variables* [19]–[21]. The boolean variable BS is introduced to represent the specification of the charging of Battery G_3 from PV G_2. Battery *can be* charged from G_2 even if commercial power source G_1 is unhealthy. This specification is not represented only with the boolean variable g_3. On the other hand, EV G_4 is *never charged* if commercial power source G_1 is unhealthy. In order to fully represent the different specifications of charging, we introduced BS to Battery G_3. In addition to these, we define the boolean variables s_i ($i = 1, \ldots, 11$) to represent the operating status of switches S_i, which are called the *control variables* [19]–[21]. The condition $s_i = 0$ (or 1) implies that S_i is open (or close). The boolean variables nl, $c\ell$, and ℓ are also defined to represent the powering condition of loads NL, CL, and L: for example, $c\ell = 1$ (or 0) implies that CL is powered (or not powered).

3.2.1 Environment

At first, we introduce the five specifications on the environment φ_e. The first specification is that in order to make the powering feasible in the target building microgrid, at least one of the three power sources—commercial power source G_1, Battery G_3 and BS, EV G_4—need to be always health. This is described in φ_{e1} with the following LTL specification:

$$\Box\{g_1 = 1 \vee (g_3 = 1 \wedge BS = 1) \vee g_4 = 1\}. \quad (2)$$

The second specification is based on a simple assumption that we make for commercial power source G_1, PV G_2, and Battery G_3: once a power source becomes unhealthy due to failure, it will remain unhealthy. This is due to a practical constraint that they need long-term repairing. The specification is described in φ_{e2} as follows:

$$\Box \bigwedge_{i=1}^{3} \{(g_i = 0) \rightarrow (\bigcirc g_i = 0)\}. \quad (3)$$

The third to fifth specifications are related to physical constraints of the charging status of Battery G_3. If Battery becomes unhealthy ($g_3 = 0$), and its charging becomes impossible due to capacity ($BS = 0$), then we hold the value of BS at 0. This specification is described in φ_{e3} as follows:

$$\Box\{(g_3 = 0 \wedge BS = 0) \rightarrow (\bigcirc BS = 0)\}. \quad (4)$$

Also, if Battery becomes unhealthy ($g_3 = 0$), then the SOC of Battery is maintained. This implies that there is no self-discharge of Battery (when it does not exchange power). This specification is described in φ_{e4} as follows:

$$\Box\{(g_3 = 0 \wedge BS = 1) \rightarrow (\bigcirc BS = 1)\}. \quad (5)$$

Finally, if commercial power source G_1 is unhealthy ($g_1 = 0$), PV is unhealthy ($g_2 = 0$), and the SOC of Battery is below the lower limit of the available range ($BS = 0$), then it is impossible for Battery to charge power from PV. Thus, we hold the value of BS at 0. This specification is described in φ_{e5} as follows:

$$\Box\{(g_1 = 0 \wedge g_2 = 0 \wedge BS = 0) \rightarrow (\bigcirc BS = 0)\}. \quad (6)$$

In summary, the environment specification φ_e is given by

$$\varphi_e = \varphi_{e1} \wedge \varphi_{e2} \wedge \varphi_{e3} \wedge \varphi_{e4} \wedge \varphi_{e5}.$$

3.2.2 System Requirements

Next, we introduce a series of specifications φ_s on the system requirements. For the use of reactive control, it is necessary that the states of environment and control satisfy the one-to-one correspondence, implying that the resultant reactive controller represented as a finite automaton should be decidable [18], [28]. As seen in Sect. 2.2, to guarantee the continuous supply of power to the most critical load CL, we describe the specification to make a supply route to the most critical load CL. Now, let us take the route from commercial power source G_1 to CL as an example. The route from G_1 to CL always holds if G_1 is health and the switch S_{11} is closed. This is described in φ_{s1} with the following LTL specification:

$$\Box\{(g_1 = 1 \wedge s_{11} = 1) \rightarrow (c\ell = 1)\}. \quad (7a)$$

The other routes to CL are described in the same manner as follows:

$$\Box\{(g_2 = 1 \wedge s_1 = 1) \rightarrow (c\ell = 1)\}, \quad (7b)$$

$$\Box\{((g_3 = 1 \wedge BS = 1) \wedge s_6 = 1) \rightarrow (c\ell = 1)\}, \quad (7c)$$

$$\Box\{(g_4 = 1 \wedge s_8 = 1 \wedge s_{10} = 1) \rightarrow (c\ell = 1)\}, \quad (7d)$$

$$\Box\{(g_4 = 1 \wedge s_8 = 1 \wedge s_7 = 1) \rightarrow (c\ell = 1)\}. \quad (7e)$$

Note that there are the two routes from EV to CL. Similar specifications are provided for L and NL. Please refer to Appendix B. The second specification in φ_s is that if a power source is healthy, then the switch connecting to it should be closed. This is trivial for making it feasible to supply power from the source. It is described with φ_{s2} as the conjunction of the following six LTL specifications (8b)–(8f):

$$\Box\{(g_1 = 1) \rightarrow (s_{11} = 1)\}, \quad (8a)$$

$$\Box\{(g_1 = 1 \wedge g_2 = 1) \rightarrow (s_1 = 1 \wedge s_2 = 0)\}, \quad (8b)$$

$$\Box\{(g_1 = 1 \wedge (g_3 = 1 \wedge BS = 1)) \rightarrow (s_3 = 1 \\ \wedge s_4 = 0 \wedge s_5 = 1 \wedge s_6 = 0)\}, \quad (8c)$$

$$\Box\{(g_1 = 1 \wedge g_3 = 0) \rightarrow (s_3 = 0 \wedge s_4 = 1 \\ \wedge s_5 = 1 \wedge s_6 = 0)\}, \quad (8d)$$

$$\Box\{(g_1 = 1 \wedge (g_3 = 1 \wedge BS = 0)) \rightarrow (s_3 = 1 \\ \wedge s_4 = 1 \wedge s_5 = 1 \wedge s_6 = 0)\}, \quad (8e)$$

$$\Box\{(g_1 = 1 \wedge g_4 = 1) \rightarrow (s_7 = 0 \wedge s_8 = 1 \\ \wedge s_9 = 0 \wedge s_{10} = 1)\}. \quad (8f)$$

In (8b), commercial power source G_1 and PV G_2 are healthy. Thus, switch S_1 is closed and switch S_2 is opened to use power supplied from PV maximally as described in (vi) of Sect. 2.2. In (8c), Battery bypasses power to NL. To do so, S_5 is closed and S_6 is opened. In (8d), because Battery G_3 is unhealthy, Battery cannot bypass power and commercial power source supplies power to NL by closing S_4. In (8e), if the SOC of Battery is insufficient ($BS = 0$), then Battery is necessary to charge. Thus, commercial power source G_1 supplies power to NL instead of Battery. In (8f), if commercial power source G_1 is healthy, then EV is connected to the grid for charging or discharging.

The third specification in φ_s is that if commercial power source G_1 is unhealthy, then any distributed power source in the grid is disconnected from G_1 as seen in (iii) of Sect. 2.2. For this, we control switches S_1, S_3, S_4, S_5, S_{10}, and S_{11} by the following LTL specification φ_{s3}:

$$\Box\{(g_1 = 0) \rightarrow (s_1 = 0 \wedge s_3 = 0 \wedge s_4 = 0 \\ \wedge s_5 = 0 \wedge s_{10} = 0 \wedge s_{11} = 0)\}. \quad (9a)$$

Also, if commercial power source G_1 is unhealthy and another power source G_i ($i = 2, \ldots, 4$) is healthy, then switches S_2, S_6, S_7, S_8, and S_9 are controlled for charging Battery G_3 or powering CL and L. This is the specification to realize the power supply to the loads according to their ranking. Note that NL is exclusive in the tripped case according to

the ranking of load importance. This control is formulated in the following set of LTL specifications:

$$\square\{((g_1 = 0) \wedge (g_2 = 1 \wedge g_3 = 1)) \rightarrow (s_2 = 1)\}, \quad (9\mathrm{b})$$

$$\square\{((g_1 = 0) \wedge (g_3 = 1 \wedge BS = 1)) \rightarrow (s_6 = 1)\}, \quad (9\mathrm{c})$$

$$\square\{(g_1 = 0 \wedge (g_3 = 1 \wedge BS = 1) \wedge g_4 = 1)$$
$$\rightarrow (s_7 = 0 \wedge s_8 = 1 \wedge s_9 = 1)\}, \quad (9\mathrm{d})$$

$$\square\{(g_1 = 0 \wedge (g_3 = 0 \vee BS = 0) \wedge g_4 = 1)$$
$$\rightarrow (s_7 = 1 \wedge s_8 = 1 \wedge s_9 = 0)\}. \quad (9\mathrm{e})$$

In (9b), if both PV G_2 and Battery G_3 are healthy, then S_2 is closed. This is from (vi) in Sect. 2.2. In (9c), if G_3 is healthy and the SOC of Battery is within the available range, then S_6 is closed. This is from (i) and (ii) in Sect. 2.2. Thus, G_3 supplies power to CL. In (9d), if EV G_4 is healthy in addition to (9c), then S_7 is opened, and S_8 and S_9 are closed. Because both G_3 and G_4 are healthy, G_3 supplies power to CL and G_4 to L. This is from (iv) in Sect. 2.2. In (9e), S_7 and S_8 are closed, and S_9 is opened. In this case, different from (9d), G_3 is unhealthy, and thus G_4 supplies power to CL. Thus, depending on which power source is healthy, it is possible to determine the supply routes to CL and L. Below, we will use φ_{s3} to represent the conjunction of the five LTL specifications (9a)–(9e).

The forth specification is opposite to the second one and is that if a power source is unhealthy, then the switch connecting to it should be opened. This is required in (vii) of Sect. 2.2. It is formulated as φ_{s4} of the conjunction of the following four LTL specifications (10a)–(10d):

$$\square\{(g_2 = 0) \rightarrow (s_1 = 0 \wedge s_2 = 0)\}, \quad (10\mathrm{a})$$

$$\square\{(g_3 = 0) \rightarrow (s_2 = 0 \wedge s_3 = 0 \wedge s_6 = 0)\}, \quad (10\mathrm{b})$$

$$\square\{(g_4 = 0) \rightarrow (s_7 = 0 \wedge s_8 = 0 \wedge s_9 = 0$$
$$\wedge s_{10} = 0)\}, \quad (10\mathrm{c})$$

$$\square\{(BS = 0) \rightarrow (s_6 = 0)\}. \quad (10\mathrm{d})$$

Note that the specification on $g_1 = 0$ has been described in φ_{s3}. In (10a), if G_2 is unhealthy, then S_1 and S_2 is opened. This is from (vii) of Sect. 2.2. In (10b), if G_3 is unhealthy, then S_2, S_3, and S_6 are opened. This is also from (vii) of Sect. 2.2 and for sending power from the other power source to CL instead of Battery. Note that S_5 is not opened because supplying power from commercial power source to NL. In (10c), if G_4 is unhealthy, then S_7, S_8, S_9, and S_{10} are opened. This is also from (vii) of Sect. 2.2, and switches S_7 and S_9 are opened to prevent the flow of power into EV from CL and L. In (10d), if the SOC of battery is not within the available range ($BS = 0$), then S_6 is opened. This is because Battery need to charge and cannot supply power during $BS = 0$.

In summary, we have the following specification φ_s of the system requirements:

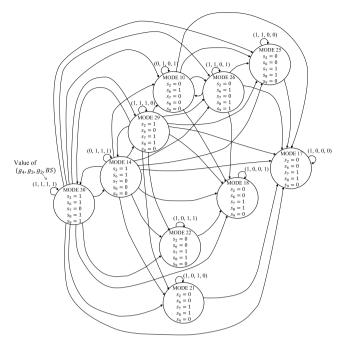$$\varphi_s = \varphi_{s1} \wedge \varphi_{s2} \wedge \varphi_{s3} \wedge \varphi_{s4}.$$

Fig. 2 Generated automaton of reactive management system under $g_1 = 0$. It has the ten control modes determined by the environment variables (g_4, g_3, g_2, BS).

Table 2 Truth table of reactive management system generated from LTL specifications. This describes the control rule of switches under the trip of commercial power source, that is, $g_1 = 0$.

MODE	g_4	g_3	g_2	BS	s_2	s_6	s_7	s_8	s_9
10	0	1	0	1	0	1	0	0	0
14	0	1	1	1	1	1	0	0	0
17	1	0	0	0	0	0	1	1	0
18	1	0	0	1	0	0	1	1	0
21	1	0	1	0	0	0	1	1	0
22	1	0	1	1	0	0	1	1	0
25	1	1	0	0	0	0	1	1	0
26	1	1	0	1	0	1	0	1	1
29	1	1	1	0	1	0	1	1	0
30	1	1	1	1	1	1	0	1	1

3.3 Synthesis Result

The LTL proposition $\varphi = \varphi_e \rightarrow \varphi_s$ provided above satisfies the GR(1) property that is applicable to an automatic generation tool of reactive system synthesis. Thus, we can generate by `Tulip` [29] a finite-state automaton (transition system) that describes the control rule of on/off status of the switches satisfying the specifications. The generated automaton under $g_1 = 0$ is shown in Fig. 2, and the truth table is shown in Table 2. Mode in the table is defined as a set of values of the environment variables and control variables, and indicates how the reactive system responds to changes of the environment for archiving reliable power supply to the critical loads.

An example of the control rule represented by the automaton is shown in Fig. 3. The transition of mode occurs from (a) to (b). In (a) with MODE10, because commercial
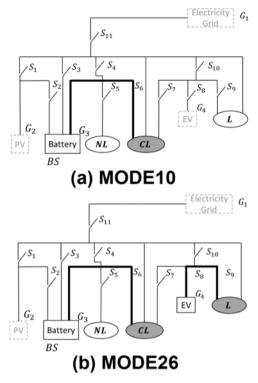
Fig. 3 Example of control rule of switches shown in Table 2. The *thick* lines represent the synthesized routes of power from source to load. The power sources encompassed by the *dotted* lines are unhealthy. In MODE10, PV G_2 and EV G_4 are unhealthy. Battery supplies power to CL. In MODE26, both Battery G_3 and EV G_4 are healthy. Thus, Battery supplies power to CL, and EV does power to L.
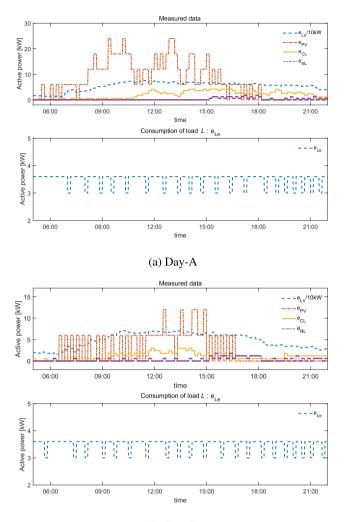

(a) Day-A

(b) Day-B

Fig. 4 Time-series data on power consumed by loads and generated by photovoltaic generation unit. The data are based on measured data in the practical office building [25] and presented for different two days, denoted as Day-A and Day-B. The label e_{Ln} stands for the consumption of load L at the healthy situation of G_1, e_{PV} for the generation of PV G_2, e_{CL} for the consumption of CL at the healthy situation of G_1, e_{NL} for that of NL, and e_{Le} for that of L at the unhealthy situation of G_1.

power source, PV, and EV are unhealthy, power is supplied to CL from Battery. Here, L is not powered according to the ranking of load importance. Now, suppose that EV becomes healthy because it arrives at the building. Then, the transition of mode occurs from MODE10 to MODE26, and power is supplied to both CL and L. Here, EV supplies power to the second important load L. This shows that the synthesized reactive BEMS handles a change of the environment variables and achieves reliable power supply to the critical loads.

4. Numerical Experiment

In this section, we conduct numerical experiments of the reactive management system synthesized in Sect. 3 using mathematical models and measured data in practice.

4.1 Measurement Data in Practical Office Building

The first set of measurement data is provided from the practical office building [25]. The set includes time-series of demand [kWh] in loads of the building and generation [kWh] in the PV unit. The dataset is shown in Fig. 4 and from 5:00 to 21:59 with equal-sampling of 10 minutes. The dataset is taken from two days with different time-series of PV generation and power demand, which we denote by Day-A and

Day-B. The weather on Day-A was partly cloudy, and the weather on Day-B was partly rainy. Thus, we evaluate the performance of the reactive BEMS with two quantitatively-different data on PV generation. Note that the time-series of power [kW] in the figure are derived from the original demand data [kWh]. In the following simulations under a situation that commercial power source G_1 is healthy, the dataset is used for the three loads CL, NL, and L, and PV G_2. We denote by $e_{\mathrm{Ln}}(t)$ the consumption of L for the healthy situation of G_1. In the figure, $e_{\mathrm{Le}}(t)$ corresponds to a steady part of the time-series $e_{\mathrm{Ln}}(t)$ and is required even if commercial power source is unhealthy. We will use $e_{\mathrm{Le}}(t)$ for numerical simulations when G_1 is unhealthy. The consumption of load L in Fig. 1 thus changes depending on whether G_1 is healthy or not. The consumption of L, denoted as $e_{\mathrm{L}}(t)$, is described as follows
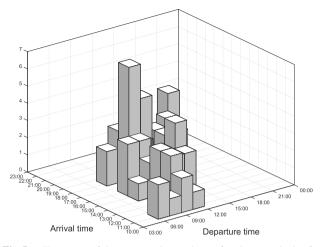
Fig. 5 Histogram of departure and arrival time for electric vehicles for company use, which is based on the practical measurement in the V2X demonstration project at Osaka, Japan.

$$e_{\mathrm{L}}(t) = g_1(t)e_{\mathrm{Ln}}(t) + (1 - g_1(t))e_{\mathrm{Le}}(t). \qquad (11)$$

The same assumption holds for CL and NL. At the unhealthy situation of G_1, CL consumes constant power of 4 kW (called $e_{\mathrm{CLe}}(t)$) based on the measurement data in the practical office building, and NL does not consume power based on the specification in the practical office building. In addition, we assume that for the unhealthy situation of G_1, the maximum output power of G_2 is restricted due to its autonomous operation, which output is normally smaller than grid-connected operation. In the practical office building, the maximum output power is 5.5 kW. Unfortunately, we have no practical data on power consumption of a control server as CPU of BEMS, and hence we do not consider the amount of power consumed in CPU.

4.2 Measurement Data in V2X Demonstration Project

The second set of measurement data is on practical utilization of EVs. We used GPS-based records of EV movement for company use and associated data on SOC of batteries, which were collected in the V2X demonstration project at Osaka Business Park (OBP) in Japan [30]–[32]. The project focused on automobiles (EV/Plug-in Hybrid Vehicle (PHV)) owned by companies in the OBP and developed a regional EMS that realized multiple functions: mitigation of the impact of charging from multiple EV/PHVs, suppression of the loading peak by coordinated use of EV/PHVs, demand response at the regional scale, and supply of energy under emergency situation.

From the measurement data, we extracted onsets at which an EV departed and arrived its owned company. Then, we plotted the result by the technique in [33] (called SDAT) as shown in Fig. 5. Also, we extracted the SOC of the plotted EV at every sampling instance of the measurement. The frequency of timezone pairs (Departure time and Arrival time) in Fig. 5 was calculated. In Fig. 5, the highest bar with frequency of 7 is the pair of time-zones of the departure

Table 3 Seven profiles of movement of electric vehicles extracted from measurement data of the V2X demonstration project at Osaka, Japan

Data No.	Departure time	Arrival time	Initial w_{EV} [kWh]	w_{EV} at arrival time [kWh]
1	10:30	17:10	14.56	11.2
2	9:40	16:40	6.64	13.28
3	9:30	17:20	13.2	9.36
4	10:30	17:30	10.24	8.16
5	9:50	16:40	14.72	9.84
6	9:40	16:40	11.04	10.48
7	10:00	16:50	15.52	12.0

in 8:58–10:35 and the arrival in 16:26–17:36. The second highest bar with frequency of 5 is the pair of time-zones of the departure in 10:35–12:11 and the arrival in 16:26–17:36. The frequencies of the other bars are from 1 to 3. Although depending on the type of business, many company cars are expected to behave in a similar manner as above; they leave companies in the early morning and return to them in the late afternoon. This is why we use the data in numerical experiments for our reactive energy management system. The data of the most frequent time zones, that is, the highest bar in Fig. 5, were chosen as the departure and arrival time in the following simulations. As the result of data analysis, we identified seven profiles of EV movement as shown in Table 3. The term "Initial w_{EV} [kWh]" represents the value of stored energy w_{EV} of in-vehicle battery at the initial time and was set as the stored energy at around 5:00 AM in the measured data. The term "w_{EV} at arrival time [kWh]" represents the value of w_{EV} at the arrival time, and its values in the table were determined by the measured data. We recall that the value of "Initial w_{EV} [kWh]" corresponds to the value of stored energy in EV at 5:00 AM, which is regarded as the beginning of the day. In that setting, the corresponding EV was charged from 5:00 AM to the departure time, thus the value of stored energy at the departure time is larger than the initial value. As a result, the value of stored energy at the arrival time possibly becomes larger than its initial value, which depends on the use of EV outside the building.

4.3 Simulation Procedure

We describe the simulation procedure of power flows in the building microgrid and charging states of the two batteries: Battery and EV. For model development, it is assumed that the power distribution lines are static and lossless, and that dynamic characteristics of the grid-connected inverters in PV, Battery, and EV are not considered. This is relevant because the dynamics of lines and inverters are so fast in micro-second order and are not dominant in time scales of our interest in this paper—hourly-order changes of power flows in the microgrid.

First of all, we introduce variables of power flows and stored energies. The variables p_{PV}, p_{EV}, p_{B}, and p_0 represent output power from PV, EV, Battery, and commercial power source, respectively. In addition, w_{B} represents the stored energy in Battery. Also, we introduce the variables p_{CL}, p_{L}, and p_{NL} to represent power flowing into loads CL, L, and NL.

In the following simulations, we introduce the constraint on the output power p_{PV} as follows:

$$0 \le p_{PV}(t) \le g_1(t)\overline{P}_{PVn} + (1 - g_1(t))\overline{P}_{PVe}. \quad (12)$$

This is based on the number of power conditioners installed in the office building. The parameter $\overline{P}_{PVn}$ represents the limit of power conditioner when commercial power source is healthy, and $\overline{P}_{PVe}$ does the limit of power conditioner when commercial power source is unhealthy. The value of $\overline{P}_{PVn}$ is set as 33 kW and $\overline{P}_{PVe}$ as 5.5 kW. Note that the rating of PV is 30 kW in the building. As mentioned in Sect. 4.1, since only one power conditioner is capable of autonomous operation, PV can output power only up to $\overline{P}_{PVe}$ under a situation that commercial power source is unhealthy.

The environment variables g_1, g_2, and g_3 are given as external signals or data. In order to generate time changes of the environmental variables g_4 and BS, the following constraints are introduced:

$$0.07W_{B,rate} \le w_B(t) \le W_{B,rate}, \quad (13)$$
$$0.3W_{EV,rate} \le w_{EV}(t) \le W_{EV,rate} \quad (14)$$

where $W_{B,rate}$ (or $W_{EV,rate}$) stands for the rated capacity of Battery (or EV). The value of $W_{B,rate}$ is set as 9.6 kWh and $W_{EV,rate}$ as 16.0 kWh based on the practical data. Here, $0.07W_{B,rate}$ and $0.3W_{EV,rate}$ represent the lower limits of available capacity that are based on practical implementations. If $w_B(t)$ satisfies the constraint (13), then the value of the environment variable BS is set to 1; otherwise, it is set to 0. Since $w_{EV}(t)$ is related to EV, the constraint (14) holds only if an EV arrives the building. The arrival of EV is determined using the EV profile data in Table 3. Thus, if $w_{EV}(t)$ satisfies the constraint (14), then the value of the environment variable g_4 is set to 1.

For given data on the environment variables above, $(e_{Ln}(t), e_{PV}(t), e_{CL}(t), e_{NL}(t), e_{Le}(t))$ in Fig. 4, and $e_{CLe}(t)$, it is possible to compute time changes of the variables $(p_0(t), p_{CL}(t), p_L(t), p_{NL}(t), p_{PV}(t), p_{EV}(t), p_B(t))$ in power flows and of charging states $(w_B(t), w_{EV}(t))$ of the batteries. The details of the computation are presented in Appendix C. We do not include the charging/discharging efficiency of batteries in the computation. The charging/discharging efficiency of batteries highly depends on SOC an temperature surrounding the batteries. Unfortunately, there is no practical data on the charging/discharging efficiency of batteries, and hence its inclusion is in future work.

In the following simulations, the time when commercial power source becomes unhealthy is set as one hour or two hours before the arrival time in Table 3. Note that $w_B(t)$ is maintained at $W_{B,rate} = 9.6$ kWh under a situation that commercial power source is healthy. This condition is based on the use of battery in the practical office building and is for simplicity of the experiments.
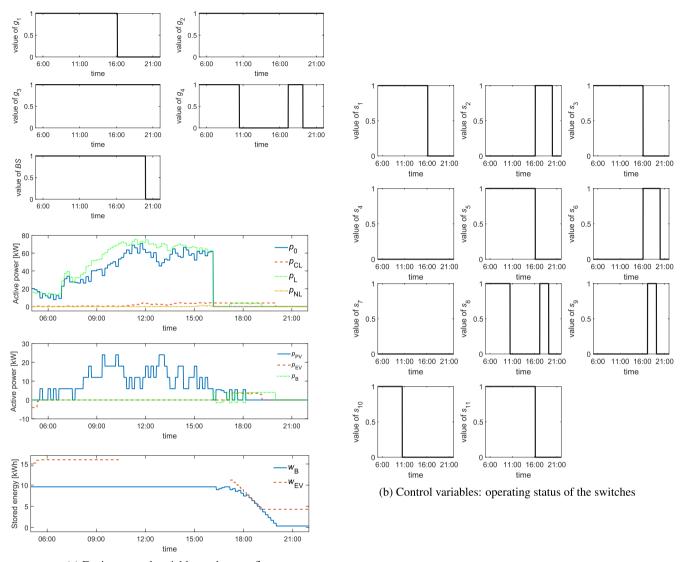
4.4 Simulation Results and Discussion

First of all, we present an example of time changes of power flows and charging states under the reactive BEMS. Figures 6(a) and 6(b) show the simulation results of power flows and charging states using No.1 data as EV profile and Day-A data in Fig. 4. The first to third rows of Fig. 6(a) show the time changes of the environment variables. The forth row shows the time changes of power supply in commercial power source and the sum of the power flowing into each load. The fifth row shows the time changes of power outputs in PV, EV, and Battery. The sixth row shows the time changes of charging states of the batteries. Figure 6(b) shows the time changes of the control variables that represent the operating status of the eleven switches and react to the above environment changes. In Figs. 6(a) and 6(b), EV starts charging at 5:00AM and leaves at the departure time 10:30AM (namely, g_4 becomes zero). After this, commercial power source is tripped at 16:10. While EV leaves the building, Battery supplies power to the critical load CL by opening switch S_5 and closing S_6. EV arrives at 17:10 and then supplies power to the second critical load L by closing switches S_8 and S_9. That is, the mode transition occurs at 17:10 from MODE 14 to MODE30. At 19:10, the stored energy $w_{EV}(t)$ falls below the lower limit of the constraint (14) so that the environment variable g_4 becomes zero. Finally, at 20:00 the stored energy $w_B(t)$ falls below the lower limit of the constraint (13). No power is therefore supplied to CL after that time.

Next, as a performance evaluation, we consider the duration of continuous power supply to the critical loads. The simulation results on Day-A and Day-B data are presented in Fig. 7. The figures (A1) and (B1) (or (A2) and (B2)) show the results when commercial power source is tripped 1 hour (or 2 hour) before the arrival time of EV. We explain the meaning of labels in Fig. 7. The labels indicate the duration when power is supplied to load CL or L under a tripped situation. The label "CL powered (w/o control)" indicates the duration if switches S_7, S_8, and S_9 are not controlled, implying the case where the reactive BEMS is not introduced in the building. Also, the label "CL powered (w/ control)" indicates the duration if the reactive BEMS is introduced, and the label "L powered (w/ control)" does the duration if the reactive BEMS is introduced.

Now, we focus on Figs. 7(A1) and (A2) on Day-A. In the synthesized reactive BEMS, the duration of continuous power supply to CL is extended with EV. Precisely saying, if $BS = 0$ holds, then EV starts to supply power to CL by controlling switches S_7, S_8, and S_9. The figures show that the durations "CL powered (w/o control)" and "CL powered (w/ control)" are the same. Because Day-A is partly cloudy, the amount of generated power from PV is enough to charging Battery so that $BS = 1$ holds during most of the day, and the amount of w_{EV} at the arrival time is not sufficiently larger than w_B of Battery G_3 (for example, see Fig. 6(a)). Therefore, no difference appears for the duration of continuous power supply to CL with and without BEMS. Also, without BEMS, L is never powered because no control of the switches is conducted. In the figures (A1) and (A2) with BEMS, however, we see that L is powered with EV by controlling the switches.

(a) Environmental variables and power flows

(b) Control variables: operating status of the switches

Fig. 6 Simulation of BEMS performance No.1 data in Table 3 as EV profile and Day-A data as power demand and PV output. In the figure (a), the first to third rows show the time changes of environment variables; the forth row the time changes of power supply from commercial power and the sum of the power flowing into each load; the fifth row the time changes of power outputs in PV, EV, and Battery; and the sixth row the time changes of charging states of the batteries. The figure (b) shows the time changes of the operating status of the eleven switches that reacted to changes of the environment.

Next, we focus on Figs. 7(B1) and (B2) on Day-B. Day-B is partly rainy, and hence the amount of generated power from PV is not enough to activating Battery so that $BS = 0$ holds at early evening of the day (please see the onset when the duration "CL powered (w/o control)" is terminated). Also, the amount of w_{EV} at the arrival time is sufficient to powering L or CL. Thus, we expect in the synthesized BEMS that EV works for keeping powering to CL instead of Battery. Indeed, it is shown in the figures (B1) and (B2) that the duration "CL powered (w/ control)" is longer than "CL powered (w/o control)". For example, in case of No.1 in (B1) the duration of continuous power supply to CL is extended by 10 minutes. For this extension, after EV arrives the building, it firstly supplies to power L and then to CL depending

on the charging state of Battery and the stored energy of EV. This is realized with the control rule of switches described by the generated automaton in Fig. 2. We numerically show that the synthesized reactive BEMS works for reliable power supply to the critical loads.

5. Conclusion

This paper reported synthesis of reactive BEMS with EV using the formal method and its numerical experiments based on measurement data in a practical office building and EV profile in a practical demonstration project. The synthesis part of this paper is an application of the methodology and tool developed in [19]–[21] to a novel control problem on
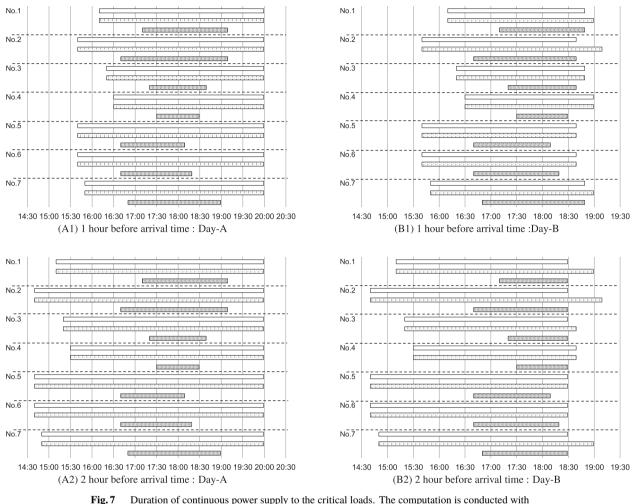
Fig. 7 Duration of continuous power supply to the critical loads. The computation is conducted with No.1 to 7 data in Table 3 and Day-A or Day-B data in Fig. 4. The figures (A1) and (B1) (or (A2) and (B2)) show the results that commercial power source is tripped 1 hour (or 2 hours) before the arrival time.

BEMS with utilization of EV. In the evaluation part, we conducted numerical experiments of the synthesized BEMS using practically-measured data in the practical office building and a V2G demonstration project in Japan. A series of numerical experiments of power flows in the microgrid was presented with measurement data on generation and load as well as EV movement. This shows that the synthesized BEMS extends the duration for supplying power to the critical load *CL* and enables power supply to *L* when commercial power source is tripped. Thus, we show that the reactive BEMS works as designed and effectively for extending the duration of continuous power supply to the most critical load.

Several follow-up studies of the work are possible. Firstly, we need to consider a case where power sources eventually return to healthy because it is of technological importance to reconnect them to the distribution network. In particular, it is of practically importance to include a requirement of return to the healthy condition of commercial power source. Also, it is of technological interest to design

a control method for extending the duration of continuous power supply to the critical loads. Regarding this, it is necessary to develop a detailed model of dynamic simulations including characteristics of power sources such the charging/discharging efficiency of batteries. In addition, for a scale of building energy systems, a large number of components coexist and thus cause a potential error in LTL specifications. We speculate that this type of potential error can be avoided with the physical protection system such as circuit breakers and relays. In this sense, it becomes significant to explore an integrated design of a logic system like this paper and a physical system for more reliable energy management of the building microgrid.

Acknowledgements

References

[1] D. Wijayasekara, O. Linda, M. Manic, and C. Rieger, "Mining building energy management system data using fuzzy anomaly detection and linguistic descriptions," IEEE Trans. Ind. Informat., vol.10, no.3, pp.1829–1840, Aug. 2014. DOI: 10.1109/TII.2014.2328291

[2] M. Manic, D. Wijayasekara, K. Amarasinghe, and J.J. Rodriguez-Andina, "Building energy management systems: The age of intelligent and adaptive buildings," IEEE Ind. Electron. Mag., vol.10, no.1, pp.25–39, March 2016. DOI: 10.1109/MIE.2015.2513749

[3] J. Machowski, J.W. Bialek, and J.R. Bumby, eds., Power System Dynamics and Stability, Wiley, England, 1997.

[4] K. Moslehi and R. Kumar, "A reliability perspective of the smart grid," IEEE Trans. Smart Grid, vol.1, no.1, pp.57–64, June 2010. DOI: 10.1109/TSG.2010.2046346

[5] T. Teratani, "Future vision through 25 years for automobiles," J. IEEJ, vol.134, no.2, pp.68–71, Feb. 2014 (in Japanese). DOI: 10.1541/ieej-journal.134.68

[6] A. Ipakchi and F. Albuyeh, "Grid of the future," IEEE Power Energy Mag., vol.7, no.2 pp.52–62, March-April 2009. DOI: 10.1109/MPE.2008.931384

[7] D. Corbus, M. Kuss, D. Piwko, G. Hinkle, M. Matsuura, M. McNeff, L. Roose, and A. Brooks, "All options on the table: Energy systems integration on the island of Maui," IEEE Power Energy Mag., vol.11 no.5, pp.65–74, Sept.-Oct. 2013. DOI: 10.1109/MPE.2013.2268814

[8] S. Negarestani, M. Fotuhi-Firuzabad, M. Rastegar, and A. Rajabi-Ghahnavieh, "Optimal sizing of storage system in a fast charging station for plug-in hybrid electric vehicles," IEEE Trans. Transport. Electrific., vol.2, no.4, pp.443–453, Dec. 2016. DOI: 10.1109/TTE.2016.2559165

[9] D. Jayaweera, "Security enhancement with nodal criticality-based integration of strategic micro grids," IEEE Trans. Power Syst., vol.30, no.1, pp.337–345, Jan. 2015. DOI: 10.1109/TPWRS.2014.2327120

[10] W. Kempton and J. Tomić, "Vehicle-to-grid power fundamentals: Calculating capacity and net revenue," J. Power Sources, vol.144, no.1, pp.268–279, June 2005. DOI: 10.1016/j.jpowsour.2004.12.025

[11] W. Kempton and J. Tomić, "Vehicle-to-grid power implementation: From stabilizing the grid to supporting large-scale renewable energy," J. Power Sources, vol.144, no.1, pp.280–294, June 2005. DOI: 10.1016/j.jpowsour.2004.12.022

[12] J. Tomić and W. Kempton, "Using fleets of electric-drive vehicles for grid support," J. Power Sources, vol.168, no.2, pp.459–468, June 2007. DOI: 10.1016/j.jpowsour.2007.03.010

[13] K. Nandha Kumar, B. Sivaneasan, P.H. Cheah, P.L. So, and D.Z. W. Wang, "V2G capacity estimation using dynamic EV scheduling," IEEE Trans. Smart Grid, vol.5, no.2, pp.1051–1060, March 2014. DOI: 10.1109/TSG.2013.2279681

[14] T. Sousa, H. Morais, Z. Vale, P. Faria, and J. Soares, "Intelligent energy resource management considering vehicle-to-grid: A simulated annealing approach," IEEE Trans. Smart Grid, vol.3, no.1, pp.535–542, March 2012. DOI: 10.1109/TSG.2011.2165303

[15] T. Suzuki, S. Inagaki, A. Kawashima, and A. Ito, "Perspective of future energy management using in-vehicle batteries," J. SICE, vol.55, no.7, pp.579–584, July 2016 (in Japanese). DOI: 10.11499/sicejl.55.579

[16] J. Voas and K. Schaffer, "Insights on formal methods in cybersecurity," Computer, vol.49, no.5, pp.102–105, May 2016. DOI: 10.1109/MC.2016.131

[17] S. Patil, G. Zhabelova, V. Vyatkin, and B. McMillin, "Towards formal verification of smart grid distributed intelligence: FREEDM case,"

[18] Proc. 41st Conf. of the IEEE industrial Electronics Society (IECON), pp.3974–3979, Yokohama, Japan, Nov. 2015. DOI: 10.1109/IECON.2015.7392719

[18] C. Baier and J.-P. Katoen, Principles of Model checking, MIT Press, England, 2008.

[19] H. Xu, U. Topcu, and R.M. Murray, "A case study on reactive protocols for aircraft electric power distribution," Proc. 51st Annual Conf. on Decision and Control, pp.1124–1129, Maui, HI, USA, Dec. 2012. DOI: 10.1109/CDC.2012.6426175

[20] H. Xu, "Design, specification, and synthesis of aircraft electric power systems control logic," PhD thesis, California Institute of Technology, March 2013. Record Number: CaltechTHESIS:05312013 - 103940337

[21] H. Xu, U. Topcu, and R.M. Murray, "Specification and synthesis of reactive protocols for aircraft electric power distribution," IEEE Trans. Control Netw. Syst., vol.2, no.2, pp.193–203, June 2015. DOI: 10.1109/TCNS.2015.2401174

[22] Z. Manna and A. Pnueli, Temporal Verification of Reactive Systems Safety, Springer-Verlag, New York, 1995.

[23] T. Saito, Y. Susuki, and T. Hikihara, "Mode switching control for output leveling of in-home electric power system: Experiment and performance evaluation," IEICE Trans. Fundamentals (Japanese Edition), vol.J100-A, no.5, pp.183–194, May 2017.

[24] Y. Susuki, T. Saito, H. Hoshino, and T. Hikihara, "Synthesis and real-time simulation of reactive controller for hot-water supply in a safety-critical hospital environment," Proc. IEEE CCTA 2017, pp.211–216, Kohala Coast, Hawai'i, Aug. 2017.

[25] M. Hiraoka, M. Koike, and M. Kamiya, "The headquater and research and development site of OMRON HEALTHCARE Co., Ltd.," Applications of Heat Pump, no.84, pp.18–23, Sept. 2012 (in Japanese).

[26] T. Ishikawa and Y. Imai, "Outline of islanding detection technology," IEEJ Trans. Power and Energy, vol.116, no.5, pp.521–524, May 1996 (in Japanese). DOI: 10.1541/ieejpes1990.116.5_521

[27] J. Rocabert, A. Luna, F. Blaabjerg, and P. Rodríguez, "Control of power converters in AC microgrids," IEEE Trans. Power Electron., vol.27, no.11 pp.4734–4749, Nov. 2012. DOI: 10.1109/TPEL.2012.2199334

[28] R. Bloem, B. Jobstmann, N. Piterman, A. Pnueli and Y. Sa'ar, "Synthesis of reactive(1) designs," J. Comput. Syst. Sci., vol.78, no.3, pp.911–938, May 2012. DOI: 10.1016/j.jcss.2011.08.007

[29] T. Wongpiromsarn, U. Topcu, N. Ozay, H. Xu, and R.M. Murray, "TuLip: A software toolbox for receding horizon temporal logic planning," Proc. 14th International Conference on Hybrid Systems: Computation and Control, pp.313–314, April 2011. DOI: 10.1145/1967701.1967747

[30] Y. Suzuki, T. Shimizu, and A. Ishigame, "Approach to the V2X(Vehicle to X) in Osaka Business Park(Part1)," 33rd Conf. on IEIEJ, A-1, Hokkaido, Japan, Sept. 2015 (in Japanese).

[31] T. Shimizu, Y. Suzuki, and A. Ishigame, "Approach to the V2X(Vehicle to X) in Osaka Business Park(Part2)," 33rd Conf. on IEIEJ, A-2, Hokkaido, Japan, Sept. 2015 (in Japanese).

[32] T. Shimizu, Y. Suzuki, and A. Ishigame, "Approach to the V2X(Vehicle to X) in Osaka Business Park(Part3)," 34th Conf. on IEIEJ, C-23, Okayama, Japan, Sept. 2016 (in Japanese).

[33] T. Yamaguchi, A. Kawashima, A. Ito, S. Inagaki, and T. Suzuki, "Real-time prediction for future profile of car travel based on statistical data and greedy algorithm," SICE J. Control, Measurement, and System Integration, vol.8, no.1, pp.7–14, Jan. 2015. DOI: 10.9746/jcmsi.8.7

Appendix A: Syntax of LTL

In this appendix, we explain Linear Temporal Logic (LTL) based on [18]–[21]. LTL is a form used in software engineering to verify the correctness of sequence of discrete states

including the temporal concept [18]. This paper uses the following LTL symbols and notations. LTL's main building block is the atomic proposition, which is a statement on a valuation of variables that has a unique truth value. LTL combines logical connectives as shown below: $\neg$: negation, $\vee$: disjunction, $\wedge$: conjunction, $\rightarrow$: implication, and $\leftrightarrow$: equivalence. In addition to the above standard symbols, symbols representing temporal operators are used in LTL. Here, let us use φ to represent a given proposition. $\bigcirc$ represents next; $\bigcirc\varphi$ signifies at the next time instant φ is true. $\square$ represents always; $\square\varphi$ signifies at all times φ is true.

Appendix B: Specifications of Power Routes to L and NL

In this appendix, we describe the specifications from the power sources to L and NL. This is described with the following LTL specification:

$$\square\{(g_1 = 1 \wedge s_{11} = 1) \rightarrow (\ell = 1)\},$$
$$\square\{(g_2 = 1 \wedge s_1 = 1) \rightarrow (\ell = 1)\},$$
$$\square\{(g_4 = 1 \wedge s_8 = 1 \wedge s_{10} = 1) \rightarrow (\ell = 1)\},$$
$$\square\{(g_4 = 1 \wedge s_8 = 1 \wedge s_9 = 1) \rightarrow (\ell = 1)\},$$
$$\square\{((g_3 = 1 \wedge BS = 1) \wedge s_5 = 1) \rightarrow (n\ell = 1)\},$$
$$\square\{(g_1 = 1 \wedge s_{11} = 1 \wedge s_4 = 1 \wedge s_5 = 1)$$
$$\rightarrow (n\ell = 1)\}.$$

Appendix C: Details of Computation in Sect. 4

In this appendix, we describe how to numerically compute the power flows and charging states of the batteries. Below, we hold the values of g_2 and g_3 at 1, and assume that EV does not discharge at the healthy situation of G_1. This is for simplicity of the performance evaluation.

$$p_{\text{PV}}(t) = g_1(t)e_{\text{PV}}(t) + p_{\text{PVB}}(t),$$

$$p_{\text{PVB}}(t) = \begin{cases} (1 - g_1(t))\overline{P}_{\text{PVe}} \\ \quad \text{if } \overline{P}_{\text{PVe}} \leq e_{\text{PV}}(t) < (6\,\text{h}^{-1})(W_{\text{B,rate}} \\ \quad - w_{\text{B}}(t)) + e_{\text{CLe}}(t), \\ (1 - g_1(t))(6\,\text{h}^{-1})(W_{\text{B,rate}} - w_{\text{B}}(t)) \\ \quad + e_{\text{CLe}}(t) \\ \quad \text{if } (6\,\text{h}^{-1})(W_{\text{B,rate}} - w_{\text{B}}(t)) \\ \quad + e_{\text{CLe}}(t) \leq e_{\text{PV}}(t) < \overline{P}_{\text{PVe}}, \\ \min\{(1 - g_1(t))\overline{P}_{\text{PVe}}, (1 - g_1(t))(6\,\text{h}^{-1}) \\ \quad \times(W_{\text{B,rate}} - w_{\text{B}}(t)) + e_{\text{CLe}}(t)\} \\ \quad \text{if } \overline{P}_{\text{PVe}} \leq e_{\text{PV}}(t) \text{ and } (6\,\text{h}^{-1}) \\ \quad \times(W_{\text{B,rate}} - w_{\text{B}}(t)) + e_{\text{CLe}}(t) \leq e_{\text{PV}}(t), \\ (1 - g_1(t))e_{\text{PV}}(t) \\ \quad \text{(otherwise)}, \end{cases}$$

$$p_{\text{EV}}(t) = -p_{\text{EVG}}(t) + (1 - g_1(t))g_4(t)\{BS(t)e_{\text{Le}}(t) \\ + (1 - BS(t))e_{\text{CLe}}(t)\},$$

$$p_{\text{EVG}}(t) = \begin{cases} g_4(t)g_1(t)(4.0\,\text{kW}) \\ \quad \text{if } 4.0\,\text{kW} \leq (6\,\text{h}^{-1})(W_{\text{EV,rate}} - w_{\text{EV}}(t)), \\ g_4(t)g_1(t)(6\,\text{h}^{-1})(W_{\text{EV,rate}} - w_{\text{EV}}(t)) \\ \quad \text{(otherwise)}, \end{cases}$$

$$p_{\text{B}}(t) = BS(t)(1 - g_1(t))e_{\text{CLe(t)}} - p_{\text{PVB}}(t),$$

$$p_0(t) = g_1(t)\{-e_{\text{PV}}(t) + e_{\text{NL}}(t) + e_{\text{CL}}(t) + e_{\text{Ln}}(t)\} \\ + p_{\text{EVG}}(t),$$

$$p_{\text{CL}}(t) = g_1(t)e_{\text{CL}}(t) + (1 - g_1(t))\{1 - (1 - BS(t)) \\ \times(1 - g_4(t))\}e_{\text{CLe}}(t),$$

$$p_{\text{L}}(t) = g_1(t)e_{\text{Ln}}(t) + (1 - g_1(t))BS(t)g_4(t)e_{\text{Le}}(t),$$

$$p_{\text{NL}}(t) = g_1(t)e_{\text{NL}},$$

$$w_{\text{B}}(t + 1) = w_{\text{B}}(t) - \left(\frac{10}{60}\,\text{h}\right)p_{\text{B}}(t),$$

$$w_{\text{EV}}(t + 1) = w_{\text{EV}}(t) - \left(\frac{10}{60}\,\text{h}\right)p_{\text{EV}}(t).$$

Shoko Kimura received her bachelor and master degrees in engineering from Osaka Prefecture University, Osaka, Japan in 2014 and 2016. She is working toward her Ph.D. degree on electrical and information systems. Her research interests are in power and energy systems. She is a member of IEEJ.

Yoshihiko Susuki received his Ph.D. degree in electrical engineering from Kyoto University, Kyoto, Japan in 2005. In 2005–2016, he was a faculty of the Department of Electrical Engineering, Kyoto University. In 2016, he joined to the Department of Electrical and Information Systems, Osaka Prefecture University, where he is currently an Associate Professor. In 2008–2010, he was a Visiting Researcher at the Department of Mechanical Engineering, University of California, Santa Barbara, under JSPS Postdoctoral Fellowship for Research Abroad. His research interests are in power and energy systems, applied nonlinear dynamics, and control applications. He is now an Associate Editor of NOLTA, IEICE and a member of IEEJ, IEEE, SIAM, and so on.

Atsushi Ishigame   received his Ph.D. degree in electrical engineering from Osaka Prefecture University, Osaka, Japan in 1993. Since 1993, he has been a faculty of the Department of Electrical Engineering, Osaka Prefecture University, where he is currently a Professor. In 1995–1996, he was a Visiting Scholar at the School of Electrical Engineering, Cornell University. His research interests are in power and energy systems, system optimization and control applications. He is a member of IEEJ, IEEE, IEIEJ and so on.